Published for SISSA by Springer

Received: December 20, 2012
Accepted: January 28, 2013
Published: February 19, 2013

Measurement of the cross-section for $Z \to e^+e^-$ production in pp collisions at $\sqrt{s} = 7\,\text{TeV}$

The LHCb collaboration

E-mail: drw1@cam.ac.uk

Abstract: A measurement of the cross-section for $pp \to Z \to e^+e^-$ is presented using data at $\sqrt{s} = 7\,\text{TeV}$ corresponding to an integrated luminosity of $0.94\,\text{fb}^{-1}$. The process is measured within the kinematic acceptance $p_T > 20\,\text{GeV}/c$ and $2 < \eta < 4.5$ for the daughter electrons and dielectron invariant mass in the range 60–120 GeV/c^2. The cross-section is determined to be

$$\sigma(pp \to Z \to e^+e^-) = 76.0 \pm 0.8 \pm 2.0 \pm 2.6\,\text{pb}$$

where the first uncertainty is statistical, the second is systematic and the third is the uncertainty in the luminosity. The measurement is performed as a function of Z rapidity and as a function of an angular variable which is closely related to the Z transverse momentum. The results are compared with previous LHCb measurements and with theoretical predictions from QCD.

Keywords: Electroweak interaction, Hadron-Hadron Scattering, QCD

ArXiv ePrint: 1212.4620

doi:10.1007/JHEP02(2013)106

JHEP02(2013)106

Contents

1 Introduction 1

2 LHCb detector 2

3 Event selection 3

4 Cross-section determination 5

5 Results 8

6 Summary 11

A Correlation matrices 13

The LHCb collaboration 16

JHEP02(2013)106

1 Introduction

The measurement of vector boson production permits a number of tests of electroweak physics and of quantum chromodynamics (QCD) to be performed. In particular, the angular acceptance of LHCb, roughly $2 < \eta < 5$ in the case of the main tracking system where η denotes pseudorapidity, complements that of the general purpose detectors ATLAS and CMS. LHCb measurements provide sensitivity to the proton structure functions at very low Bjorken x values where the parton distribution functions (PDFs) are not particularly well constrained by previous data from HERA (see for example ref. [1]).

The most straightforward decay modes in which the $W^{\pm}$ and Z bosons can be studied using the LHCb data are the muonic channels, $Z \to \mu^+\mu^-$ and $W^+ \to \mu^+\nu_\mu$. Measurements of $Z \to \mu^+\mu^-$ and of $Z \to \tau^+\tau^-$ using the LHCb data at $\sqrt{s} = 7\,\text{TeV}$ have already been presented [2, 3]. To complement these studies, the electron channels $Z \to e^+e^-$ and $W^+ \to e^+\nu_e$, which offer statistically independent samples with different sources of systematic uncertainties, are examined.

The main difficulty with electron[1] reconstruction in LHCb is the energy measurement. A significant amount of material is traversed by the electrons before they reach the momentum analysing magnet, and their measured momenta are therefore liable to be reduced by bremsstrahlung. For low energy electrons, the bremsstrahlung photons can frequently be identified in the electromagnetic calorimeter and their energies added to the measured momentum of the electron. However, in the case of $W^{\pm}$ and Z decays, the electrons are of high momentum and transverse momentum (p_{T}), so that the bremsstrahlung photons often

[1]The term "electron" is used generically to refer to either e^+ or e^-.

overlap with the electrons. The LHCb calorimeters were designed so as to optimise the the measurement of photons and π^0s from heavy flavour decays, whose transverse energy ($E_{\rm T}$) values are generally well below 10 GeV. As a consequence, individual calorimeter cells saturate at $E_{\rm T}$ around 10 GeV, so it is not possible to substitute the calorimeter energy for the momentum measured using the spectrometer. We therefore have a situation in which the electron directions are well determined, but their energies are underestimated by a variable amount, typically around 25%. Nevertheless, the available information can be used to study certain interesting variables.

In this paper, we present a measurement of the cross-section for $\rm pp \to Z \to e^+e^-$ using the data recorded by LHCb in 2011 at $\sqrt{s} = 7$ TeV. Throughout this paper we use $\rm Z \to e^+e^-$ to refer to the process $\rm Z/\gamma^* \to e^+e^-$ where either a virtual photon or a Z boson is produced and decays to $\rm e^+e^-$. For consistency, the measurement is presented in the same kinematic region as the recent measurement of $\rm Z \to \mu^+\mu^-$ using the 2010 LHCb data at $\sqrt{s} = 7$ TeV [2]: $2 < \eta < 4.5$ and $p_{\rm T} > 20\,{\rm GeV}/c$ for the leptons and $60 < M < 120\,{\rm GeV}/c^2$ for the dileptons where M is the invariant mass. Since the rapidity of the Z boson can be determined to a precision of ∼0.05, the rapidity distribution will be presented. However, the $p_{\rm T}$ of the Z boson is poorly determined and its distribution will not be discussed. A similar problem was encountered by the D0 collaboration [4], who employed a new variable proposed in ref. [5] depending only on track angles

$$\phi^* \equiv \tan\left(\frac{\phi_{\rm acop}}{2}\right) \Big/ \cosh\left(\frac{\Delta\eta}{2}\right) \approx \frac{p_{\rm T}}{Mc}\,, \tag{1.1}$$

where M and $p_{\rm T}$ refer to the lepton pair, $\Delta\eta$ and $\Delta\phi$ are the differences in pseudorapidity and azimuthal angles respectively between the leptons, and the acoplanarity angle is $\phi_{\rm acop} = \pi - |\Delta\phi|$. The $p_{\rm T}$ of the Z boson is correlated with ϕ^*, and the resolution on ϕ^* is excellent, with a precision better than 0.001. The measurement of ϕ^* presented here therefore largely accesses the same physics as a measurement of the Z $p_{\rm T}$ distribution. The measurement of the distribution of Z rapidity (denoted $y_{\rm Z}$) is expected to show sensitivity to the choice of PDFs, while ϕ^* is likely to be more sensitive to higher order effects in the QCD modelling.

After a brief description of the detector, section 3 describes the event selection, and section 4 outlines the determination of the cross-section. The results are given in section 5 followed by a short summary.

2 LHCb detector

The LHCb detector [6] is a single-arm forward spectrometer covering the pseudorapidity range $2 < \eta < 5$, designed primarily for the study of particles containing b or c quarks. The detector includes a high precision tracking system consisting of a silicon-strip vertex detector surrounding the pp interaction region, a large-area silicon-strip detector located upstream of a dipole magnet with a bending power of about 4 Tm, and three stations of silicon-strip detectors and straw drift tubes placed downstream. The combined tracking system has a momentum resolution $\Delta p/p$ that varies from 0.4% at 5 GeV/c to 0.6%

JHEP02(2013)106

at 100 GeV/c for hadrons and muons, and an impact parameter resolution of 20 μm for tracks with high transverse momentum. Charged hadrons are identified using two ring-imaging Cherenkov detectors. Photon, electron and hadron candidates are identified by a calorimeter system consisting of scintillating-pad (SPD) and preshower (PRS) detectors, an electromagnetic calorimeter (ECAL) and a hadronic calorimeter (HCAL). The acceptance of the calorimeter system is roughly $1.8 < \eta < 4.3$. Muons are identified by a system composed of alternating layers of iron and multiwire proportional chambers.

The trigger [7] consists of a hardware stage, based on information from the calorimeter and muon systems, followed by a software stage which applies full event reconstruction. A significant improvement to the trigger was implemented during August 2011 which affected the trigger efficiency for $\mathrm{Z} \to \mathrm{e}^+\mathrm{e}^-$. The data samples before and after this change are treated separately and will be referred to as data sample I and data sample II. These correspond to integrated luminosities of $581 \pm 20\,\mathrm{pb}^{-1}$ and $364 \pm 13\,\mathrm{pb}^{-1}$ respectively, yielding a total of $945 \pm 33\,\mathrm{pb}^{-1}$.

3 Event selection

The $\mathrm{Z} \to \mathrm{e}^+\mathrm{e}^-$ sample is initially selected by single-electron triggers, which require electrons to have an E_T above a given threshold between 10 and 15 GeV depending on the data-taking period and specific trigger. The $\mathrm{Z} \to \mathrm{e}^+\mathrm{e}^-$ selection starts from a sample of $\mathrm{e}^+\mathrm{e}^-$ candidates with high invariant mass, which is refined by requiring the following selection criteria:

- At least one of the candidate electrons must be selected by a high-E_T electron trigger.
- The electrons are both required to have $p_\mathrm{T} > 20\,\mathrm{GeV}/c$ and pseudorapidity in the range $2.0 < \eta < 4.5$. The invariant mass of the $\mathrm{e}^+\mathrm{e}^-$ pair should be greater than $40\,\mathrm{GeV}/c^2$.
- Requirements on calorimeter information are imposed to provide particle identification (PID) of electrons. The particle must satisfy $E_\mathrm{ECAL}/pc > 0.1$, where p is the particle momentum, with bremsstrahlung correction if available, and E_ECAL is the ECAL energy associated with the particle. The particle is required to lie within the HCAL acceptance and to satisfy $E_\mathrm{HCAL}/pc < 0.05$, where E_HCAL is the HCAL energy associated with the particle. The energy in the preshower detector associated with the particle is required to satisfy $E_\mathrm{PRS} > 50\,\mathrm{MeV}$. These requirements impose an electromagnetic shower profile, while being loose enough to maintain a high electron efficiency despite the effects of calorimeter saturation and bremsstrahlung.
- If more than one $\mathrm{Z} \to \mathrm{e}^+\mathrm{e}^-$ candidate satisfies the above requirements in an event, just one candidate is used, chosen at random. This only affects around 0.5% of cases, and in all instances the multiple candidates share one daughter.

A sample of same-sign $\mathrm{e}^\pm\mathrm{e}^\pm$ combinations, subject to the same selection criteria, is used to provide a data-based estimate of background. The main background is expected to arise from hadrons that shower early in the ECAL and consequently fake the signature of

JHEP02(2013)106

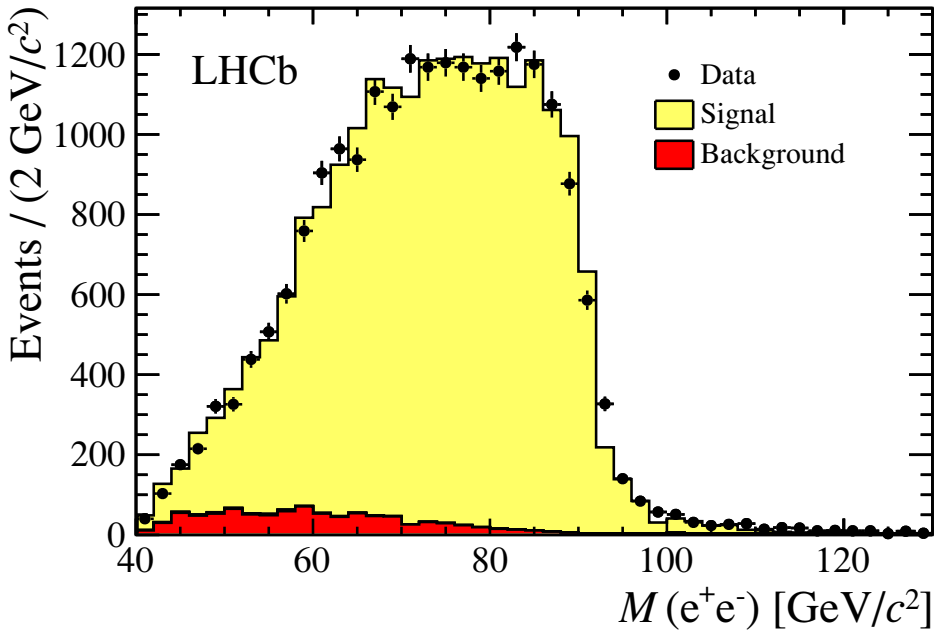

Figure 1. Invariant mass distribution of $Z \to e^+e^-$ candidates. The data are shown as points with error bars, the background obtained from same-sign data is shown in red (dark shading), to which the expectation from signal simulation is added in yellow (light shading). The $Z \to e^+e^-$ simulated distribution has been normalised to the (background-subtracted) data.

an electron. These will contribute approximately equally to same-sign and opposite-sign pairs. The contribution from semileptonic heavy flavour decays should be similar to the small level ($\sim 0.2\%$) estimated for the $Z \to \mu^+\mu^-$ channel [2]; in any case, subtracting the same-sign contribution should account for most of this effect.

Simulated event samples of $Z \to e^+e^-$ with $M(e^+e^-) > 40\,\mathrm{GeV}/c^2$ are also used to assess some efficiencies as discussed below. Simulated samples of $Z \to \tau^+\tau^-$ and of $t\bar{t}$ are used to assess possible background contributions. For the simulation, pp collisions are generated using Pythia 6.4 [8] with a specific LHCb configuration [9] and the CTEQ6L1 PDF set [10]. The interaction of the generated particles with the detector and its response are implemented using the Geant4 toolkit [11, 12] as described in ref. [13]. Simulated samples based on different versions of GEANT and of the detector model are employed, which allows the reliability of the simulation to be assessed. The simulated events are then reconstructed in the same way as the data, including simulation of the relevant trigger conditions.

The invariant mass distribution of the selected candidates is shown in figure 1. The distribution falls off abruptly above the Z mass and is spread to lower masses by bremsstrahlung. Good agreement in shape is observed between data and the simulation sample used in the data correction; this will be further discussed below. The background estimated from same-sign events amounts to 4.5% of the total number of e^+e^- candidates. The backgrounds from $\tau^+\tau^-$ and $t\bar{t}$ events are estimated to be around 0.1% and are neglected.

JHEP02(2013)106

	Data sample I	Data sample II
$\int \mathcal{L}dt$ [pb^{-1}]	581 ± 20	364 ± 13
$\epsilon_{\rm GEC}$	0.947 ± 0.004	
$\epsilon_{\rm trig}$	0.715 ± 0.021	0.899 ± 0.003
$\epsilon_{\rm track}$	0.913 ± 0.015	
$\epsilon_{\rm kin}$	0.500 ± 0.007	
$\epsilon_{\rm PID}$	0.844 ± 0.011	
$f_{\rm FSR}$	1.049 ± 0.005	
$f_{\rm MZ}$	0.967 ± 0.001	

Table 1. Quantities entering into the cross-section determination, averaged over the range of Z rapidity used.

4 Cross-section determination

In a given bin of Z rapidity or ϕ^*, the cross-section is calculated using

$$\sigma(\mathrm{pp} \to \mathrm{Z} \to \mathrm{e^+e^-}) = \frac{\mathrm{N(e^+e^-)} - \mathrm{N(e^\pm e^\pm)}}{\epsilon_{\rm GEC} \cdot \epsilon_{\rm trig} \cdot \epsilon_{\rm track} \cdot \epsilon_{\rm kin} \cdot \epsilon_{\rm PID} \cdot \int \mathcal{L}\mathrm{dt}} \cdot \mathrm{f_{FSR}} \cdot \mathrm{f_{MZ}} \ , \tag{4.1}$$

where $N(\mathrm{e^+e^-})$ is the number of Z candidates selected in data, $N(\mathrm{e^\pm e^\pm})$ is the background estimated from the number of same-sign candidates and $\int \mathcal{L}dt$ is the integrated luminosity. The cross-section $\sigma(\mathrm{pp} \to \mathrm{Z} \to \mathrm{e^+e^-})$ denotes the product of the inclusive production cross-section for the Z or γ^* and the branching ratio to $\mathrm{e^+e^-}$. The meaning and estimation of the other factors are described below. The values obtained for each, averaged over the acceptance, are summarised in table 1.

The luminosity is determined as described in ref. [14] and has an uncertainty of 3.5%. The factor $f_{\rm FSR}$ accounts for the effects of final-state electromagnetic radiation, correcting the measurement to the Born level. As in the $\mathrm{Z} \to \mu^+\mu^-$ analysis [2] it is determined using PHOTOS [15] interfaced to PYTHIA [8], with HORACE [16] used as a cross-check. An overall systematic uncertainty of 0.5% is assigned to this correction [17]. The factor $f_{\rm MZ}$ corrects for $\mathrm{e^+e^-}$ events outside the mass range $60 < M(\mathrm{e^+e^-}) < 120\,\mathrm{GeV}$ which pass the event selection, and is estimated from simulation by examining the true mass for selected events.

The probability for a $\mathrm{Z} \to \mathrm{e^+e^-}$ event to satisfy the trigger and selection requirements is given by the product of the efficiency factors, ϵ, as described below.

- Global event cuts (GEC) are applied in the trigger in order to prevent very large events from dominating the processing time. Their efficiency for selecting signal events is given by $\epsilon_{\rm GEC}$. In the $\mathrm{Z} \to \mathrm{e^+e^-}$ case, the most important requirement is on the multiplicity of SPD hits, $N_{\rm SPD} \leq 600$. This is strongly correlated with the number of primary vertices reconstructed in the event. The inefficiency is assessed by comparing with $\mathrm{Z} \to \mu^+\mu^-$ candidates recorded in the same running period using a dimuon trigger for which a less stringent requirement of 900 hits is imposed. A

JHEP02(2013)106

correction is made for the small difference in the numbers of SPD hits associated with the electrons and muons themselves. This procedure is adopted for each number of reconstructed primary vertices and the results are combined to obtain the overall efficiency.

- The trigger efficiency for events passing the final selection, ϵ_{trig}, is determined from data. A sample of events triggered independently of the e^+ is identified and used to determine the efficiency for triggering the e^+, and likewise for the e^-. Using the total numbers of candidates for which the single electron trigger is satisfied at each stage by the e^+ (N^+), by the e^- (N^-) and by both (N^{+-}), the efficiency for triggering the e^+ is given by $\varepsilon^+ = N^{+-}/N^-$. The overall efficiency is then taken to be $\varepsilon^- + \varepsilon^+ - \varepsilon^-\varepsilon^+$ assuming that the e^+ and e^- are triggered independently. The procedure is validated on simulated events. The determination is performed separately in each bin of Z rapidity and ϕ^*. In all cases, the statistical uncertainty on the efficiency is taken as a contribution to the systematic uncertainty on the measurement.

- The track-finding efficiency, ϵ_{track}, represents the probability that both of the electrons are successfully reconstructed. The simulation is used to determine the track-finding efficiency, in bins of Z rapidity and ϕ^*, by calculating the probability that, in a $Z \to e^+e^-$ event whose generated electrons lie within the kinematic acceptance, both of the electrons are associated with reconstructed tracks that satisfy the track quality requirements, but not necessarily the kinematic requirements. Its statistical precision is propagated as a contribution to the systematic uncertainty.

  This efficiency is checked in data using a tag-and-probe approach. One electron is tagged using the standard requirements, and a search is made for an accompanying cluster of electromagnetic energy having a high E_{T} and forming a high invariant mass with the tag electron. If such a cluster has no associated track it provides evidence of a failure to reconstruct the other electron. This sample contains significant background, which can be discriminated by examining the p_{T} distribution of the tag electron for cases where the photon candidate is and is not isolated. The p_{T} distribution of the electrons in signal events in data displays a clear shoulder extending to $\sim 45\,\text{GeV}/c$ while that for background falls monotonically, as shown in figure 2. The number of signal-like events in which a cluster is not associated with a track can be used to estimate a tracking efficiency, and the ratio of efficiencies between data and simulation is applied as a correction to the tracking efficiency. The precision of the test is taken to define a systematic uncertainty, assumed to be fully correlated between bins of rapidity and ϕ^*.

- The kinematic efficiency, ϵ_{kin}, represents the probability that, in a $Z \to e^+e^-$ event whose generated electrons lie within the kinematic acceptance and are associated with reconstructed tracks, both tracks pass the kinematic selection requirements $2 < \eta < 4.5$ and $p_{\text{T}} > 20\,\text{GeV}/c$. The efficiency is estimated from simulation, with its statistical precision being treated as a contribution to the systematic uncertainty.
  This determination relies on a correct simulation, which can be tested using data. For

JHEP02(2013)106

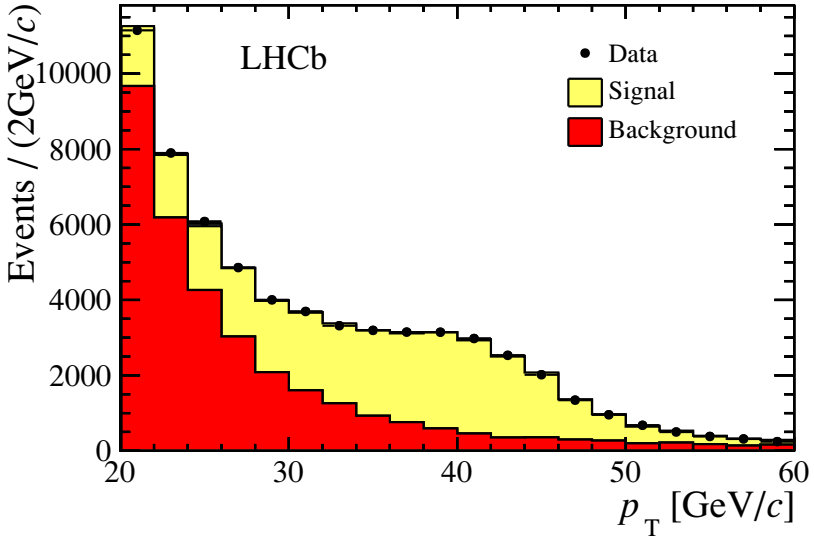

Figure 2. Distribution of $p_{\rm T}$ for the "tag" electron in cases where an isolated cluster of energy of high $E_{\rm T}$ is found in the electromagnetic calorimeter. This is fitted with two components obtained from data, the $\rm Z \to e^+e^-$ signal whose shape is taken from those candidates where the cluster is associated with an identified electron track, and background whose shape is obtained from candidates where the cluster is not isolated.

example, underestimation of the amount of material in the simulation would cause a discrepancy between data and simulation in the $p_{\rm T}$ distributions of the electrons or the reconstructed mass spectrum shown in figure 1. By comparing the shapes of the reconstructed mass spectrum and other kinematic distributions in data with different simulation samples, a systematic uncertainty on the momentum scale and hence on the kinematic efficiency is assigned. This is combined with the statistical uncertainty mentioned above, with the systematic contribution taken to be fully correlated between bins of rapidity and ϕ^*.

- The PID efficiency, $\epsilon_{\rm PID}$, represents the probability that, in a $\rm Z \to e^+e^-$ event with reconstructed electron tracks satisfying the kinematic requirements, both tracks fulfil the calorimeter energy requirements for identified electrons. This includes the probability that the tracks are within the calorimeter acceptance and have been successfully associated with calorimeter information. Because of the acceptance contribution, the efficiency has a strong dependence on the Z rapidity. This dependence is taken from simulation, while the overall normalisation of the PID efficiency is estimated directly from data, using a tag-and-probe method.
  Starting from a sample which requires just one high $p_{\rm T}$ electron, events are selected by applying the usual criteria except that only one of the $\rm e^+$ and $\rm e^-$ (the "tag") is required to pass the calorimeter-based electron identification requirements. The other track is used as a "probe" to test the PID efficiency. The requirement of only one identified electron admits a significant level of background, which is assessed similarly to the tracking efficiency by examining the $p_{\rm T}$ distribution of the tag or alternatively

JHEP02(2013)106

the p_T of the probe electron or the invariant mass of the two particles. The size of the signal component can be used to define the number of Z events which fail the PID, and hence to determine the PID efficiency and its uncertainty.

A systematic uncertainty is also assigned to the same-sign background subtraction. The assumption that same-sign $e^{\pm}e^{\pm}$ combinations model background in e^+e^- events is tested by selecting events which satisfy all criteria except that one of the particles fails the calorimeter energy requirements. This sample should be dominated by background, and shows an excess of ∼8% of opposite-sign events over same-sign events. Accordingly a systematic uncertainty amounting to 8% of the number of same-sign events is assigned to the measurements.

5 Results

Using the efficiencies described above, the event yields detailed in table 2 and eq. (4.1) separate cross-section measurements for the two data-taking periods are obtained. Since these are in good agreement, the results are combined using a weighted average, and assuming their uncertainties are fully correlated apart from the statistical contribution and the uncertainty in the trigger efficiency. Data sample II has a smaller integrated luminosity but a higher and more precisely estimated trigger efficiency. The weighting of the two samples is chosen to minimise the total uncertainty on the cross-section integrated over Z rapidity. The values of the differential cross-sections obtained are given in table 2. Correlation matrices may be found in the appendix. The bin $4.25 < y_Z < 4.5$ is empty in data, and is expected to have close to zero detection efficiency since the calorimeter acceptance extends only slightly beyond 4.25. Hence no measurement is possible. However, the QCD calculations discussed below predict a cross-section below ∼0.01 pb in this bin, which is negligibly small, so comparisons with the $Z\to \mu^+\mu^-$ results or with theoretical calculations in the range $2 < y_Z < 4.5$ are still meaningful.

The cross-section integrated over Z rapidity is obtained by summing the cross-sections of all bins of y_Z, taking the uncertainties associated with the GEC and the luminosity to be fully correlated between bins, along with parts of the tracking, kinematic and PID efficiencies, and treating the other contributions as uncorrelated. The cross-section is measured to be

$$\sigma(pp \to Z \to e^+e^-) = 76.0 \pm 0.8\,(\text{stat.}) \pm 2.0\,(\text{syst.}) \pm 2.6\,(\text{lumi.}) \pm 0.4\,(\text{FSR})\,\text{pb},$$

where the first uncertainty is statistical, the second is the experimental systematic uncertainty, the third is the luminosity uncertainty and the last represents the uncertainty in the FSR correction. Since the results have been corrected to the Born level using the factor f_{FSR}, it is possible to compare this measurement with that found in the $Z\to \mu^+\mu^-$ analysis [2] using $37\,\text{pb}^{-1}$ of data, namely $76.7 \pm 1.7\,(\text{stat.}) \pm 3.3\,(\text{syst.}) \pm 2.7\,(\text{lumi.})$ pb. Accounting for correlated uncertainties, the ratio of cross-sections is

$$\frac{\sigma(pp \to Z \to e^+e^-)}{\sigma(pp \to Z \to \mu^+\mu^-)} = 0.990 \pm 0.024\,(\text{stat.}) \pm 0.044\,(\text{syst.}).$$

JHEP02(2013)106

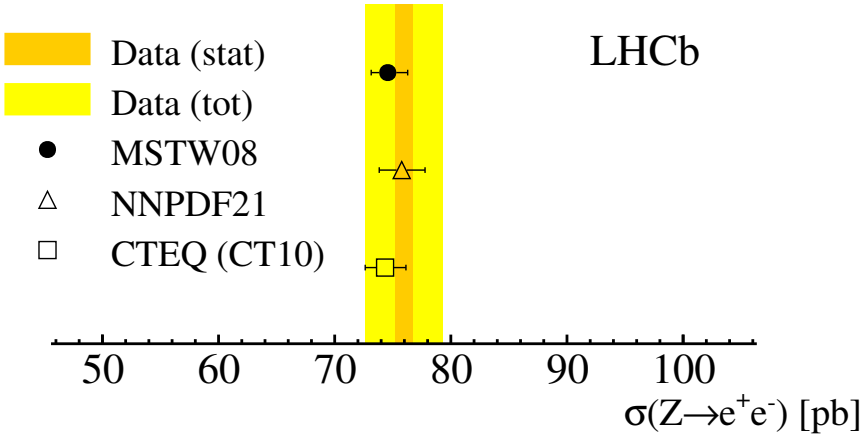

Figure 3. Cross-section for $pp \to Z \to e^+e^-$ at $\sqrt{s} = 7\,\text{TeV}$ measured in LHCb, shown as the yellow band. The inner (darker) band represents the statistical uncertainty and the outer the total uncertainty. The measurement corresponds to the kinematic acceptance, $p_T > 20\,\text{GeV}/c$ and $2 < \eta < 4.5$ for the leptons and $60 < M < 120\,\text{GeV}/c^2$ for the dilepton. The points show the various theoretical predictions with their uncertainties as described in the text.

This may be regarded as a cross-check of the analyses. Assuming lepton universality, the two cross-sections can be combined in a weighted average so as to minimise the total uncertainty, yielding

$$\sigma(pp \to Z \to \ell^+\ell^-) = 76.1 \pm 0.7\,(\text{stat.}) \pm 1.8\,(\text{syst.}) \pm 2.7\,(\text{lumi.}) \pm 0.4\,(\text{FSR})\,\text{pb}.$$

A recent measurement in $Z \to \tau^+\tau^-$ decays which has a larger statistical uncertainty [3] can also be combined with the electron and muon channels, yielding

$$\sigma(pp \to Z \to \ell^+\ell^-) = 75.4 \pm 0.8\,(\text{stat.}) \pm 1.7\,(\text{syst.}) \pm 2.6\,(\text{lumi.}) \pm 0.4\,(\text{FSR})\,\text{pb}.$$

The results may be compared with theoretical calculations similar to those used in the interpretation of the $Z \to \mu^+\mu^-$ analysis [2]. These calculations are performed at NNLO ($\mathcal{O}(\alpha_s^2)$) with the program FEWZ [18] version 2.1.1 and using the NNLO PDF sets of MSTW08 [19], NNPDF21 [20] or CTEQ (CT10 NNLO) [21, 22]. In figure 3 we present the measured cross-section and in figure 4(a) the measurements of the Z rapidity distribution, compared in each case with the three calculations. The uncertainties in the predictions include the effect of varying the renormalisation and factorisation scales by factors of two around the nominal value, which is set to the Z mass, combined in quadrature with the PDF uncertainties at 68% confidence level. The data agree with expectations within the uncertainties.

The differential cross-section as a function of ϕ^* is shown in figure 4(b), compared with the predictions of QCD to NNLO. Figure 5(a) displays the ratios of these predictions to the measurements. The NNLO calculations tend to overestimate the data at low ϕ^* and to underestimate the data at high ϕ^*. It is expected that the ϕ^* distribution, like that of p_T, is significantly affected by multiple soft gluon emissions, which are not sufficiently

JHEP02(2013)106

y_Z	$N(e^+e^-)$	$N(e^\pm e^\pm)$	$d\sigma/dy_Z$ [pb]	f_{FSR}
2.00–2.25	988	40	$13.6 \pm 0.7 \pm 0.4 \pm 0.3 \pm 0.1$	1.049 ± 0.004
2.25–2.50	3064	121	$39.4 \pm 1.0 \pm 0.6 \pm 0.8 \pm 0.2$	1.046 ± 0.002
2.50–2.75	4582	202	$56.7 \pm 1.2 \pm 0.7 \pm 1.3 \pm 0.3$	1.050 ± 0.002
2.75–3.00	5076	214	$63.2 \pm 1.3 \pm 0.8 \pm 1.5 \pm 0.3$	1.049 ± 0.002
3.00–3.25	4223	181	$59.9 \pm 1.4 \pm 0.8 \pm 1.6 \pm 0.3$	1.056 ± 0.002
3.25–3.50	2429	135	$43.8 \pm 1.3 \pm 0.8 \pm 1.1 \pm 0.2$	1.054 ± 0.003
3.50–3.75	906	61	$20.5 \pm 1.0 \pm 0.7 \pm 0.6 \pm 0.1$	1.030 ± 0.006
3.75–4.00	143	18	$5.9 \pm 0.8 \pm 0.5 \pm 0.3 \pm 0.1$	1.074 ± 0.029
4.00–4.25	9	2	$0.66 \pm 0.44 \pm 0.30 \pm 0.04 \pm 0.02$	1.074 ± 0.029
4.25–4.50	0	0	—	

ϕ^*	$N(e^+e^-)$	$N(e^\pm e^\pm)$	$d\sigma/d\phi^*$ [pb]	f_{FSR}
0.00–0.05	9696	363	$693 \pm 10 \pm 6 \pm 17 \pm 3$	1.059 ± 0.001
0.05–0.10	4787	219	$326 \pm 7 \pm 4 \pm 8 \pm 2$	1.047 ± 0.002
0.10–0.15	2382	115	$164 \pm 5 \pm 3 \pm 4 \pm 1$	1.039 ± 0.002
0.15–0.20	1384	80	$99.1 \pm 4.0 \pm 2.0 \pm 2.2 \pm 0.5$	1.043 ± 0.003
0.20–0.30	1434	82	$49.6 \pm 2.0 \pm 1.1 \pm 1.0 \pm 0.3$	1.042 ± 0.003
0.30–0.40	707	39	$25.5 \pm 1.4 \pm 0.8 \pm 0.6 \pm 0.1$	1.049 ± 0.004
0.40–0.60	583	41	$10.8 \pm 0.7 \pm 0.4 \pm 0.3 \pm 0.1$	1.052 ± 0.005
0.60–0.80	217	13	$4.05 \pm 0.38 \pm 0.20 \pm 0.09 \pm 0.03$	1.054 ± 0.005
0.80–1.00	91	9	$1.41 \pm 0.23 \pm 0.11 \pm 0.03 \pm 0.02$	1.051 ± 0.009
1.00–2.00	119	9	$0.41 \pm 0.06 \pm 0.03 \pm 0.01 \pm 0.02$	1.035 ± 0.011

Table 2. Event yields and measurements for the differential cross-section of $pp \to Z \to e^+e^-$ at $\sqrt{s}$ =7 TeV as a function of Z rapidity, y_Z, and of ϕ^*. The first uncertainty is statistical, the second and third are the uncorrelated and correlated experimental systematic uncertainties respectively, and the fourth is the uncertainty in the FSR correction. The common luminosity uncertainty of 3.5% is not explicitly included here. The results are given for the combined data sample. The right-hand column gives the values used for the FSR correction factor.

accounted for in fixed order calculations. A QCD calculation which takes this into account through resummation is provided by RESBOS [23–25].[2] Another resummed calculation [26] has been compared with ATLAS data [27] in the central region of rapidity, but is not yet available for the LHCb acceptance. Alternatively, POWHEG [28, 29] provides a framework

[2]The P branch of RESBOS is used with grids for LHC at $\sqrt{s} = 7$ TeV based on CTEQ6.6.

JHEP02(2013)106

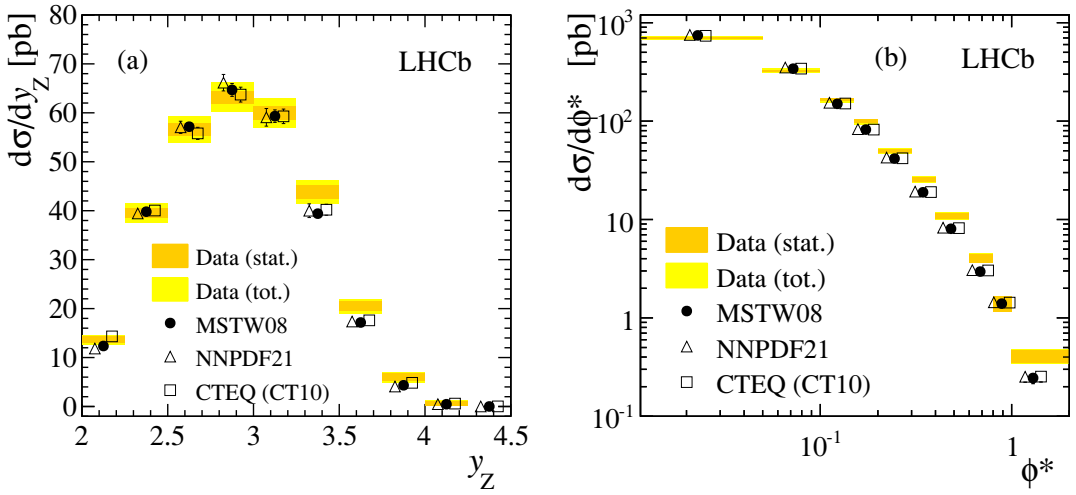

Figure 4. Differential cross-section for $pp \to Z \to e^+e^-$ as a function of (a) Z rapidity and (b) ϕ^*. The measurements based on the $\sqrt{s} = 7\,\text{TeV}$ LHCb data are shown as the yellow bands where the inner (darker) band represents the statistical uncertainty and the outer the total uncertainty. NNLO QCD predictions are shown as points with error bars reflecting their uncertainties as described in the text.

whereby a NLO QCD ($\mathcal{O}(\alpha_S)$) calculation can be interfaced to a parton shower model such as Pythia which can approximate higher order effects. Comparisons with these models, and with the LHCb version [9] of Pythia [8] are shown in figure 5(b). The Resbos and Powheg distributions are normalised to their own cross-section predictions, while the Pythia distribution is normalised to the cross-section measured in data. It is seen that Resbos gives a reasonable description of the ϕ^* distribution. Powheg shows that the combination of a parton shower with the $\mathcal{O}(\alpha_S)$ QCD prediction significantly improves the description of data in the low ϕ^* region, while in the high ϕ^* region the data are still underestimated. Pythia models the data reasonably well. Overall, Resbos and Pythia seem to be the more successful of the calculation schemes considered here.

6 Summary

A measurement of the $pp \to Z \to e^+e^-$ cross-section in pp collisions at $\sqrt{s} = 7\,\text{TeV}$ using $0.94\,\text{fb}^{-1}$ of data recorded by LHCb is presented. Although the characteristics of the LHCb detector prevent a sharp mass peak from being seen, a clean sample of events is identified with less than 5% background. Within the kinematic acceptance, $p_T > 20\,\text{GeV}/c$ and $2 < \eta < 4.5$ for the leptons and $60 < M < 120\,\text{GeV}/c^2$ for the dielectron, the cross-section is measured to be

$$\sigma(pp \to Z \to e^+e^-) = 76.0 \pm 0.8\,(\text{stat.}) \pm 2.0\,(\text{syst.}) \pm 2.6\,(\text{lumi.}) \pm 0.4\,(\text{FSR})\,\text{pb}.$$

The cross-section is also measured in bins of the rapidity of the Z and of the angular variable ϕ^*. The measurements of the rapidity distribution and of the integrated cross-sections are consistent with previous measurements using Z decays to $\mu^+\mu^-$ and $\tau^+\tau^-$

JHEP02(2013)106

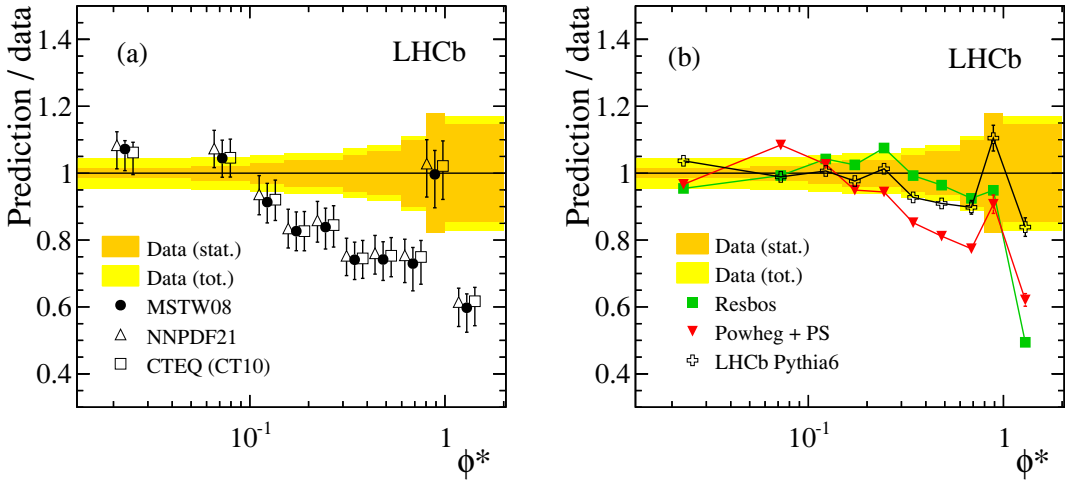

Figure 5. Ratios of various QCD calculations to data for the differential cross-section for $pp \to Z \to e^+e^-$ as a function of ϕ^*. The measurements based on the $\sqrt{s} = 7\,\text{TeV}$ LHCb data are shown as the yellow band centred at unity where the inner (darker) band represents the statistical uncertainty and the outer the total uncertainty. (a) NNLO QCD predictions shown as points with error bars reflecting their uncertainties as described in the text. Small lateral displacements of the theory points are made to improve clarity. (b) Ratios of the predictions of Pythia, Resbos and Powheg to the data shown as points, with error bars that reflect the statistical uncertainties in the predictions. For most points, these errors are so small that they are not visible.

and show good agreement with the expectations from NNLO QCD calculations. The ϕ^* distribution, related to the Z p_T distribution, is better modelled by calculations which approximately include the effects of higher orders.

Acknowledgments

We express our gratitude to our colleagues in the CERN accelerator departments for the excellent performance of the LHC. We thank the technical and administrative staff at the LHCb institutes. We acknowledge support from CERN and from the national agencies: CAPES, CNPq, FAPERJ and FINEP (Brazil); NSFC (China); CNRS/IN2P3 and Region Auvergne (France); BMBF, DFG, HGF and MPG (Germany); SFI (Ireland); INFN (Italy); FOM and NWO (The Netherlands); SCSR (Poland); ANCS/IFA (Romania); MinES, Rosatom, RFBR and NRC "Kurchatov Institute" (Russia); MinECo, XuntaGal and GENCAT (Spain); SNSF and SER (Switzerland); NAS Ukraine (Ukraine); STFC (United Kingdom); NSF (USA). We also acknowledge the support received from the ERC under FP7. The Tier1 computing centres are supported by IN2P3 (France), KIT and BMBF (Germany), INFN (Italy), NWO and SURF (The Netherlands), PIC (Spain), GridPP (United Kingdom). We are thankful for the computing resources put at our disposal by Yandex LLC (Russia), as well as to the communities behind the multiple open source software packages that we depend on.

JHEP02(2013)106

A Correlation matrices

y_Z bin	2.–2.25	2.25–2.5	2.5–2.75	2.75–3.	3.–3.25	3.25–3.5	3.5–3.75	3.75–4.	4.–4.25
2.00–2.25	1								
2.25–2.50	0.47	1							
2.50–2.75	0.50	0.70	1						
2.75–3.00	0.51	0.70	0.75	1					
3.00–3.25	0.50	0.69	0.74	0.75	1				
3.25–3.50	0.45	0.62	0.66	0.67	0.66	1			
3.50–3.75	0.35	0.49	0.52	0.52	0.51	0.46	1		
3.75–4.00	0.20	0.27	0.29	0.29	0.29	0.26	0.20	1	
4.00–4.25	0.05	0.07	0.08	0.08	0.08	0.07	0.06	0.03	1

Table 3. Correlation coefficients for the differential cross-section of $Z \to e^+e^-$ at 7 TeV between bins of Z rapidity, y_Z. Both statistical and systematic contributions are included.

ϕ^* bin	0.–0.05	0.05–0.1	0.1–0.15	0.15–0.2	0.2–0.3	0.3–0.4	0.4–0.6	0.6–0.8	0.8–1.	1.–2.
0.00–0.05	1									
0.05–0.10	0.80	1								
0.10–0.15	0.73	0.67	1							
0.15–0.20	0.63	0.58	0.53	1						
0.20–0.30	0.62	0.58	0.53	0.45	1					
0.30–0.40	0.51	0.48	0.43	0.38	0.38	1				
0.40–0.60	0.46	0.43	0.39	0.34	0.34	0.28	1			
0.60–0.80	0.34	0.31	0.29	0.25	0.25	0.20	0.18	1		
0.80–1.00	0.21	0.20	0.18	0.16	0.15	0.13	0.11	0.08	1	
1.00–2.00	0.23	0.21	0.19	0.17	0.17	0.14	0.12	0.09	0.06	1

Table 4. Correlation coefficients for the differential cross-section of $Z \to e^+e^-$ at 7 TeV between bins of ϕ^*. Both statistical and systematic contributions are included.

References

[1] R. Thorne, A. Martin, W. Stirling and G. Watt, *Parton distributions and QCD at LHCb*, arXiv:0808.1847 [INSPIRE].

[2] LHCb collaboration, *Inclusive W and Z production in the forward region at $\sqrt{s} = 7$ TeV*, *JHEP* **06** (2012) 058 [arXiv:1204.1620] [INSPIRE].

[3] LHCb collaboration, *A study of the Z production cross-section in pp collisions at $\sqrt{s} = 7$ TeV using tau final states*, *JHEP* **01** (2013) 111 [arXiv:1210.6289] [INSPIRE].

[4] D0 collaboration, V.M. Abazov et al., *Precise study of the Z/γ^* boson transverse momentum distribution in $p\bar{p}$ collisions using a novel technique*, *Phys. Rev. Lett.* **106** (2011) 122001 [arXiv:1010.0262] [INSPIRE].

JHEP02(2013)106

[5] A. Banfi, S. Redford, M. Vesterinen, P. Waller and T. Wyatt, *Optimisation of variables for studying dilepton transverse momentum distributions at hadron colliders*, *Eur. Phys. J.* **C 71** (2011) 1600 [arXiv:1009.1580] [INSPIRE].

[6] LHCb collaboration, *The LHCb detector at the LHC*, 2008 *JINST* **3** S08005 [INSPIRE].

[7] R. Aaij et al., *The LHCb trigger and its performance*, arXiv:1211.3055 [INSPIRE].

[8] T. Sjöstrand, S. Mrenna and P.Z. Skands, *PYTHIA 6.4 physics and manual*, *JHEP* **05** (2006) 026 [hep-ph/0603175] [INSPIRE].

[9] I. Belyaev et al., *Handling of the generation of primary events in* Gauss*, the LHCb simulation framework*, *IEEE Nucl. Sci. Symp. Conf. Rec.* (2010) 1155.

[10] P.M. Nadolsky et al., *Implications of CTEQ global analysis for collider observables*, *Phys. Rev.* **D 78** (2008) 013004 [arXiv:0802.0007] [INSPIRE].

[11] GEANT4 collaboration, J. Allison et al., *GEANT4 developments and applications*, *IEEE Trans. Nucl. Sci.* **53** (2006) 270.

[12] GEANT4 collaboration, S. Agostinelli et al., *GEANT4: a simulation toolkit*, *Nucl. Instrum. Meth.* **A 506** (2003) 250 [INSPIRE].

[13] M. Clemencic et al., *The LHCb simulation application, Gauss: design, evolution and experience*, *J. Phys. Conf. Ser.* **331** (2011) 032023.

[14] LHCb collaboration, *Absolute luminosity measurements with the LHCb detector at the LHC*, 2012 *JINST* **7** P01010 [arXiv:1110.2866] [INSPIRE].

[15] P. Golonka and Z. Was, *PHOTOS Monte Carlo: a precision tool for QED corrections in Z and W decays*, *Eur. Phys. J.* **C 45** (2006) 97 [hep-ph/0506026] [INSPIRE].

[16] C. Carloni Calame, G. Montagna, O. Nicrosini and A. Vicini, *Precision electroweak calculation of the production of a high transverse-momentum lepton pair at hadron colliders*, *JHEP* **10** (2007) 109 [arXiv:0710.1722] [INSPIRE].

[17] Z. Was, private communication, http://annapurna.ifj.edu.pl/∼wasm/phNLO.htm.

[18] R. Gavin, Y. Li, F. Petriello and S. Quackenbush, *FEWZ 2.0: a code for hadronic Z production at next-to-next-to-leading order*, *Comput. Phys. Commun.* **182** (2011) 2388 [arXiv:1011.3540] [INSPIRE].

[19] A. Martin, W. Stirling, R. Thorne and G. Watt, *Parton distributions for the LHC*, *Eur. Phys. J.* **C 63** (2009) 189 [arXiv:0901.0002] [INSPIRE].

[20] R.D. Ball et al., *A first unbiased global NLO determination of parton distributions and their uncertainties*, *Nucl. Phys.* **B 838** (2010) 136 [arXiv:1002.4407] [INSPIRE].

[21] H.-L. Lai et al., *New parton distributions for collider physics*, *Phys. Rev.* **D 82** (2010) 074024 [arXiv:1007.2241] [INSPIRE].

[22] P. Nadolsky et al., *Progress in CTEQ-TEA PDF analysis*, arXiv:1206.3321 [INSPIRE].

[23] G. Ladinsky and C. Yuan, *The nonperturbative regime in QCD resummation for gauge boson production at hadron colliders*, *Phys. Rev.* **D 50** (1994) 4239 [hep-ph/9311341] [INSPIRE].

[24] C. Balázs and C. Yuan, *Soft gluon effects on lepton pairs at hadron colliders*, *Phys. Rev.* **D 56** (1997) 5558 [hep-ph/9704258] [INSPIRE].

JHEP02(2013)106

[25] F. Landry, R. Brock, P.M. Nadolsky and C. Yuan, *Tevatron Run-1 Z boson data and Collins-Soper-Sterman resummation formalism*, *Phys. Rev.* **D 67** (2003) 073016 [hep-ph/0212159] [INSPIRE].

[26] A. Banfi, M. Dasgupta, S. Marzani and L. Tomlinson, *Predictions for Drell-Yan ϕ^* and Q_T observables at the LHC*, *Phys. Lett.* **B 715** (2012) 152 [arXiv:1205.4760] [INSPIRE].

[27] ATLAS collaboration, *Measurement of angular correlations in Drell-Yan lepton pairs to probe Z/γ^* boson transverse momentum at $\sqrt{s} = 7$ TeV with the ATLAS detector*, arXiv:1211.6899 [INSPIRE].

[28] S. Alioli, P. Nason, C. Oleari and E. Re, *NLO vector-boson production matched with shower in POWHEG*, *JHEP* **07** (2008) 060 [arXiv:0805.4802] [INSPIRE].

[29] S. Alioli, P. Nason, C. Oleari and E. Re, *Vector boson plus one jet production in POWHEG*, *JHEP* **01** (2011) 095 [arXiv:1009.5594] [INSPIRE].

JHEP02(2013)106

The LHCb collaboration

R. Aaij[38], C. Abellan Beteta[33,n], A. Adametz[11], B. Adeva[34], M. Adinolfi[43], C. Adrover[6], A. Affolder[49], Z. Ajaltouni[5], J. Albrecht[35], F. Alessio[35], M. Alexander[48], S. Ali[38], G. Alkhazov[27], P. Alvarez Cartelle[34], A.A. Alves Jr[22,35], S. Amato[2], Y. Amhis[7], L. Anderlini[17,f], J. Anderson[37], R. Andreassen[57], R.B. Appleby[51], O. Aquines Gutierrez[10], F. Archilli[18], A. Artamonov [32], M. Artuso[53], E. Aslanides[6], G. Auriemma[22,m], S. Bachmann[11], J.J. Back[45], C. Baesso[54], V. Balagura[28], W. Baldini[16], R.J. Barlow[51], C. Barschel[35], S. Barsuk[7], W. Barter[44], A. Bates[48], Th. Bauer[38], A. Bay[36], J. Beddow[48], I. Bediaga[1], S. Belogurov[28], K. Belous[32], I. Belyaev[28], E. Ben-Haim[8], M. Benayoun[8], G. Bencivenni[18], S. Benson[47], J. Benton[43], A. Berezhnoy[29], R. Bernet[37], M.-O. Bettler[44], M. van Beuzekom[38], A. Bien[11], S. Bifani[12], T. Bird[51], A. Bizzeti[17,h], P.M. Bjørnstad[51], T. Blake[35], F. Blanc[36], C. Blanks[50], J. Blouw[11], S. Blusk[53], A. Bobrov[31], V. Bocci[22], A. Bondar[31], N. Bondar[27], W. Bonivento[15], S. Borghi[51], A. Borgia[53], T.J.V. Bowcock[49], E. Bowen[37], C. Bozzi[16], T. Brambach[9], J. van den Brand[39], J. Bressieux[36], D. Brett[51], M. Britsch[10], T. Britton[53], N.H. Brook[43], H. Brown[49], A. Büchler-Germann[37], I. Burducea[26], A. Bursche[37], J. Buytaert[35], S. Cadeddu[15], O. Callot[7], M. Calvi[20,j], M. Calvo Gomez[33,n], A. Camboni[33], P. Campana[18,35], A. Carbone[14,c], G. Carboni[21,k], R. Cardinale[19,i], A. Cardini[15], H. Carranza-Mejia[47], L. Carson[50], K. Carvalho Akiba[2], G. Casse[49], M. Cattaneo[35], Ch. Cauet[9], M. Charles[52], Ph. Charpentier[35], P. Chen[3,36], N. Chiapolini[37], M. Chrzaszcz [23], K. Ciba[35], X. Cid Vidal[34], G. Ciezarek[50], P.E.L. Clarke[47], M. Clemencic[35], H.V. Cliff[44], J. Closier[35], C. Coca[26], V. Coco[38], J. Cogan[6], E. Cogneras[5], P. Collins[35], A. Comerma-Montells[33], A. Contu[15], A. Cook[43], M. Coombes[43], G. Corti[35], B. Couturier[35], G.A. Cowan[36], D. Craik[45], S. Cunliffe[50], R. Currie[47], C. D'Ambrosio[35], P. David[8], P.N.Y. David[38], I. De Bonis[4], K. De Bruyn[38], S. De Capua[51], M. De Cian[37], J.M. De Miranda[1], L. De Paula[2], W. De Silva[57], P. De Simone[18], D. Decamp[4], M. Deckenhoff[9], H. Degaudenzi[36,35], L. Del Buono[8], C. Deplano[15], D. Derkach[14], O. Deschamps[5], F. Dettori[39], A. Di Canto[11], J. Dickens[44], H. Dijkstra[35], P. Diniz Batista[1], M. Dogaru[26], F. Domingo Bonal[33,n], S. Donleavy[49], F. Dordei[11], A. Dosil Suárez[34], D. Dossett[45], A. Dovbnya[40], F. Dupertuis[36], R. Dzhelyadin[32], A. Dziurda[23], A. Dzyuba[27], S. Easo[46,35], U. Egede[50], V. Egorychev[28], S. Eidelman[31], D. van Eijk[38], S. Eisenhardt[47], U. Eitschberger[9], R. Ekelhof[9], L. Eklund[48], I. El Rifai[5], Ch. Elsasser[37], D. Elsby[42], A. Falabella[14,e], C. Färber[11], G. Fardell[47], C. Farinelli[38], S. Farry[12], V. Fave[36], D. Ferguson[47], V. Fernandez Albor[34], F. Ferreira Rodrigues[1], M. Ferro-Luzzi[35], S. Filippov[30], C. Fitzpatrick[35], M. Fontana[10], F. Fontanelli[19,i], R. Forty[35], O. Francisco[2], M. Frank[35], C. Frei[35], M. Frosini[17,f], S. Furcas[20], E. Furfaro[21], A. Gallas Torreira[34], D. Galli[14,c], M. Gandelman[2], P. Gandini[52], Y. Gao[3], J. Garofoli[53], P. Garosi[51], J. Garra Tico[44], L. Garrido[33], C. Gaspar[35], R. Gauld[52], E. Gersabeck[11], M. Gersabeck[51], T. Gershon[45,35], Ph. Ghez[4], V. Gibson[44], V.V. Gligorov[35], C. Göbel[54], D. Golubkov[28], A. Golutvin[50,28,35], A. Gomes[2], H. Gordon[52], M. Grabalosa Gándara[5], R. Graciani Diaz[33], L.A. Granado Cardoso[35], E. Graugés[33], G. Graziani[17], A. Grecu[26], E. Greening[52], S. Gregson[44], O. Grünberg[55], B. Gui[53], E. Gushchin[30], Yu. Guz[32], T. Gys[35], C. Hadjivasiliou[53], G. Haefeli[36], C. Haen[35], S.C. Haines[44], S. Hall[50], T. Hampson[43], S. Hansmann-Menzemer[11], N. Harnew[52], S.T. Harnew[43], J. Harrison[51], P.F. Harrison[45], T. Hartmann[55], J. He[7], V. Heijne[38], K. Hennessy[49], P. Henrard[5], J.A. Hernando Morata[34], E. van Herwijnen[35], E. Hicks[49], D. Hill[52], M. Hoballah[5], C. Hombach[51], P. Hopchev[4], W. Hulsbergen[38], P. Hunt[52], T. Huse[49], N. Hussain[52], D. Hutchcroft[49], D. Hynds[48], V. Iakovenko[41], P. Ilten[12], J. Imong[43], R. Jacobsson[35], A. Jaeger[11], E. Jans[38], F. Jansen[38], P. Jaton[36], F. Jing[3], M. John[52], D. Johnson[52], C.R. Jones[44], B. Jost[35], M. Kaballo[9], S. Kandybei[40], M. Karacson[35], T.M. Karbach[35], I.R. Kenyon[42], U. Kerzel[35], T. Ketel[39], A. Keune[36], B. Khanji[20], O. Kochebina[7], I. Komarov[36,29], R.F. Koopman[39], P. Koppenburg[38],

JHEP02(2013)106

M. Korolev[29], A. Kozlinskiy[38], L. Kravchuk[30], K. Kreplin[11], M. Kreps[45], G. Krocker[11], P. Krokovny[31], F. Kruse[9], M. Kucharczyk[20,23,j], V. Kudryavtsev[31], T. Kvaratskheliya[28,35], V.N. La Thi[36], D. Lacarrere[35], G. Lafferty[51], A. Lai[15], D. Lambert[47], R.W. Lambert[39], E. Lanciotti[35], G. Lanfranchi[18,35], C. Langenbruch[35], T. Latham[45], C. Lazzeroni[42], R. Le Gac[6], J. van Leerdam[38], J.-P. Lees[4], R. Lefèvre[5], A. Leflat[29,35], J. Lefrançois[7], O. Leroy[6], Y. Li[3], L. Li Gioi[5], M. Liles[49], R. Lindner[35], C. Linn[11], B. Liu[3], G. Liu[35], J. von Loeben[20], J.H. Lopes[2], E. Lopez Asamar[33], N. Lopez-March[36], H. Lu[3], J. Luisier[36], H. Luo[47], A. Mac Raighne[48], F. Machefert[7], I.V. Machikhiliyan[4,28], F. Maciuc[26], O. Maev[27,35], S. Malde[52], G. Manca[15,d], G. Mancinelli[6], N. Mangiafave[44], U. Marconi[14], R. Märki[36], J. Marks[11], G. Martellotti[22], A. Martens[8], L. Martin[52], A. Martín Sánchez[7], M. Martinelli[38], D. Martinez Santos[34], D. Martinez Santos[39], D. Martins Tostes[2], A. Massafferri[1], R. Matev[35], Z. Mathe[35], C. Matteuzzi[20], M. Matveev[27], E. Maurice[6], A. Mazurov[16,30,35,e], J. McCarthy[42], R. McNulty[12], B. Meadows[57,52], F. Meier[9], M. Meissner[11], M. Merk[38], D.A. Milanes[13], M.-N. Minard[4], J. Molina Rodriguez[54], S. Monteil[5], D. Moran[51], P. Morawski[23], R. Mountain[53], I. Mous[38], F. Muheim[47], K. Müller[37], R. Muresan[26], B. Muryn[24], B. Muster[36], P. Naik[43], T. Nakada[36], R. Nandakumar[46], I. Nasteva[1], M. Needham[47], N. Neufeld[35], A.D. Nguyen[36], T.D. Nguyen[36], C. Nguyen-Mau[36,o], M. Nicol[7], V. Niess[5], R. Niet[9], N. Nikitin[29], T. Nikodem[11], S. Nisar[56], A. Nomerotski[52], A. Novoselov[32], A. Oblakowska-Mucha[24], V. Obraztsov[32], S. Oggero[38], S. Ogilvy[48], O. Okhrimenko[41], R. Oldeman[15,d,35], M. Orlandea[26], J.M. Otalora Goicochea[2], P. Owen[50], B.K. Pal[53], A. Palano[13,b], M. Palutan[18], J. Panman[35], A. Papanestis[46], M. Pappagallo[48], C. Parkes[51], C.J. Parkinson[50], G. Passaleva[17], G.D. Patel[49], M. Patel[50], G.N. Patrick[46], C. Patrignani[19,i], C. Pavel-Nicorescu[26], A. Pazos Alvarez[34], A. Pellegrino[38], G. Penso[22,l], M. Pepe Altarelli[35], S. Perazzini[14,c], D.L. Perego[20,j], E. Perez Trigo[34], A. Pérez-Calero Yzquierdo[33], P. Perret[5], M. Perrin-Terrin[6], G. Pessina[20], K. Petridis[50], A. Petrolini[19,i], A. Phan[53], E. Picatoste Olloqui[33], B. Pie Valls[33], B. Pietrzyk[4], T. Pilař[45], D. Pinci[22], S. Playfer[47], M. Plo Casasus[34], F. Polci[8], G. Polok[23], A. Poluektov[45,31], E. Polycarpo[2], D. Popov[10], B. Popovici[26], C. Potterat[33], A. Powell[52], J. Prisciandaro[36], V. Pugatch[41], A. Puig Navarro[36], W. Qian[4], J.H. Rademacker[43], B. Rakotomiaramanana[36], M.S. Rangel[2], I. Raniuk[40], N. Rauschmayr[35], G. Raven[39], S. Redford[52], M.M. Reid[45], A.C. dos Reis[1], S. Ricciardi[46], A. Richards[50], K. Rinnert[49], V. Rives Molina[33], D.A. Roa Romero[5], P. Robbe[7], E. Rodrigues[51], P. Rodriguez Perez[34], G.J. Rogers[44], S. Roiser[35], V. Romanovsky[32], A. Romero Vidal[34], J. Rouvinet[36], T. Ruf[35], H. Ruiz[33], G. Sabatino[22,k], J.J. Saborido Silva[34], N. Sagidova[27], P. Sail[48], B. Saitta[15,d], C. Salzmann[37], B. Sanmartin Sedes[34], M. Sannino[19,i], R. Santacesaria[22], C. Santamarina Rios[34], E. Santovetti[21,k], M. Sapunov[6], A. Sarti[18,l], C. Satriano[22,m], A. Satta[21], M. Savrie[16,e], D. Savrina[28,29], P. Schaack[50], M. Schiller[39], H. Schindler[35], S. Schleich[9], M. Schlupp[9], M. Schmelling[10], B. Schmidt[35], O. Schneider[36], A. Schopper[35], M.-H. Schune[7], R. Schwemmer[35], B. Sciascia[18], A. Sciubba[18,l], M. Seco[34], A. Semennikov[28], K. Senderowska[24], I. Sepp[50], N. Serra[37], J. Serrano[6], P. Seyfert[11], M. Shapkin[32], I. Shapoval[40,35], P. Shatalov[28], Y. Shcheglov[27], T. Shears[49,35], L. Shekhtman[31], O. Shevchenko[40], V. Shevchenko[28], A. Shires[50], R. Silva Coutinho[45], T. Skwarnicki[53], N.A. Smith[49], E. Smith[52,46], M. Smith[51], K. Sobczak[5], M.D. Sokoloff[57], F.J.P. Soler[48], F. Soomro[18,35], D. Souza[43], B. Souza De Paula[2], B. Spaan[9], A. Sparkes[47], P. Spradlin[48], F. Stagni[35], S. Stahl[11], O. Steinkamp[37], S. Stoica[26], S. Stone[53], B. Storaci[37], M. Straticiuc[26], U. Straumann[37], V.K. Subbiah[35], S. Swientek[9], V. Syropoulos[39], M. Szczekowski[25], P. Szczypka[36,35], T. Szumlak[24], S. T'Jampens[4], M. Teklishyn[7], E. Teodorescu[26], F. Teubert[35], C. Thomas[52], E. Thomas[35], J. van Tilburg[11], V. Tisserand[4], M. Tobin[37], S. Tolk[39], D. Tonelli[35], S. Topp-Joergensen[52], N. Torr[52], E. Tournefier[4,50], S. Tourneur[36], M.T. Tran[36], M. Tresch[37], A. Tsaregorodtsev[6], P. Tsopelas[38], N. Tuning[38],

JHEP02(2013)106

M. Ubeda Garcia[35], A. Ukleja[25], D. Urner[51], U. Uwer[11], V. Vagnoni[14], G. Valenti[14], R. Vazquez Gomez[33], P. Vazquez Regueiro[34], S. Vecchi[16], J.J. Velthuis[43], M. Veltri[17,g], G. Veneziano[36], M. Vesterinen[35], B. Viaud[7], D. Vieira[2], X. Vilasis-Cardona[33,n], A. Vollhardt[37], D. Volyanskyy[10], D. Voong[43], A. Vorobyev[27], V. Vorobyev[31], C. Voß[55], H. Voss[10], R. Waldi[55], R. Wallace[12], S. Wandernoth[11], J. Wang[53], D.R. Ward[44], N.K. Watson[42], A.D. Webber[51], D. Websdale[50], M. Whitehead[45], J. Wicht[35], D. Wiedner[11], L. Wiggers[38], G. Wilkinson[52], M.P. Williams[45,46], M. Williams[50,p], F.F. Wilson[46], J. Wishahi[9], M. Witek[23], W. Witzeling[35], S.A. Wotton[44], S. Wright[44], S. Wu[3], K. Wyllie[35], Y. Xie[47,35], F. Xing[52], Z. Xing[53], Z. Yang[3], R. Young[47], X. Yuan[3], O. Yushchenko[32], M. Zangoli[14], M. Zavertyaev[10,a], F. Zhang[3], L. Zhang[53], W.C. Zhang[12], Y. Zhang[3], A. Zhelezov[11], A. Zhokhov[28], L. Zhong[3], A. Zvyagin[35]

[1] *Centro Brasileiro de Pesquisas Físicas (CBPF), Rio de Janeiro, Brazil*
[2] *Universidade Federal do Rio de Janeiro (UFRJ), Rio de Janeiro, Brazil*
[3] *Center for High Energy Physics, Tsinghua University, Beijing, China*
[4] *LAPP, Université de Savoie, CNRS/IN2P3, Annecy-Le-Vieux, France*
[5] *Clermont Université, Université Blaise Pascal, CNRS/IN2P3, LPC, Clermont-Ferrand, France*
[6] *CPPM, Aix-Marseille Université, CNRS/IN2P3, Marseille, France*
[7] *LAL, Université Paris-Sud, CNRS/IN2P3, Orsay, France*
[8] *LPNHE, Université Pierre et Marie Curie, Université Paris Diderot, CNRS/IN2P3, Paris, France*
[9] *Fakultät Physik, Technische Universität Dortmund, Dortmund, Germany*
[10] *Max-Planck-Institut für Kernphysik (MPIK), Heidelberg, Germany*
[11] *Physikalisches Institut, Ruprecht-Karls-Universität Heidelberg, Heidelberg, Germany*
[12] *School of Physics, University College Dublin, Dublin, Ireland*
[13] *Sezione INFN di Bari, Bari, Italy*
[14] *Sezione INFN di Bologna, Bologna, Italy*
[15] *Sezione INFN di Cagliari, Cagliari, Italy*
[16] *Sezione INFN di Ferrara, Ferrara, Italy*
[17] *Sezione INFN di Firenze, Firenze, Italy*
[18] *Laboratori Nazionali dell'INFN di Frascati, Frascati, Italy*
[19] *Sezione INFN di Genova, Genova, Italy*
[20] *Sezione INFN di Milano Bicocca, Milano, Italy*
[21] *Sezione INFN di Roma Tor Vergata, Roma, Italy*
[22] *Sezione INFN di Roma La Sapienza, Roma, Italy*
[23] *Henryk Niewodniczanski Institute of Nuclear Physics Polish Academy of Sciences, Kraków, Poland*
[24] *AGH University of Science and Technology, Kraków, Poland*
[25] *National Center for Nuclear Research (NCBJ), Warsaw, Poland*
[26] *Horia Hulubei National Institute of Physics and Nuclear Engineering, Bucharest-Magurele, Romania*
[27] *Petersburg Nuclear Physics Institute (PNPI), Gatchina, Russia*
[28] *Institute of Theoretical and Experimental Physics (ITEP), Moscow, Russia*
[29] *Institute of Nuclear Physics, Moscow State University (SINP MSU), Moscow, Russia*
[30] *Institute for Nuclear Research of the Russian Academy of Sciences (INR RAN), Moscow, Russia*
[31] *Budker Institute of Nuclear Physics (SB RAS) and Novosibirsk State University, Novosibirsk, Russia*
[32] *Institute for High Energy Physics (IHEP), Protvino, Russia*
[33] *Universitat de Barcelona, Barcelona, Spain*
[34] *Universidad de Santiago de Compostela, Santiago de Compostela, Spain*
[35] *European Organization for Nuclear Research (CERN), Geneva, Switzerland*
[36] *Ecole Polytechnique Fédérale de Lausanne (EPFL), Lausanne, Switzerland*
[37] *Physik-Institut, Universität Zürich, Zürich, Switzerland*
[38] *Nikhef National Institute for Subatomic Physics, Amsterdam, The Netherlands*

JHEP02(2013)106

[39] Nikhef National Institute for Subatomic Physics and VU University Amsterdam, Amsterdam, The Netherlands
[40] NSC Kharkiv Institute of Physics and Technology (NSC KIPT), Kharkiv, Ukraine
[41] Institute for Nuclear Research of the National Academy of Sciences (KINR), Kyiv, Ukraine
[42] University of Birmingham, Birmingham, United Kingdom
[43] H.H. Wills Physics Laboratory, University of Bristol, Bristol, United Kingdom
[44] Cavendish Laboratory, University of Cambridge, Cambridge, United Kingdom
[45] Department of Physics, University of Warwick, Coventry, United Kingdom
[46] STFC Rutherford Appleton Laboratory, Didcot, United Kingdom
[47] School of Physics and Astronomy, University of Edinburgh, Edinburgh, United Kingdom
[48] School of Physics and Astronomy, University of Glasgow, Glasgow, United Kingdom
[49] Oliver Lodge Laboratory, University of Liverpool, Liverpool, United Kingdom
[50] Imperial College London, London, United Kingdom
[51] School of Physics and Astronomy, University of Manchester, Manchester, United Kingdom
[52] Department of Physics, University of Oxford, Oxford, United Kingdom
[53] Syracuse University, Syracuse, NY, United States
[54] Pontifícia Universidade Católica do Rio de Janeiro (PUC-Rio), Rio de Janeiro, Brazil, associated to[2]
[55] Institut für Physik, Universität Rostock, Rostock, Germany, associated to[11]
[56] Institute of Information Technology, COMSATS, Lahore, Pakistan, associated to[53]
[57] University of Cincinnati, Cincinnati, OH, United States, associated to[53]

[a] P.N. Lebedev Physical Institute, Russian Academy of Science (LPI RAS), Moscow, Russia
[b] Università di Bari, Bari, Italy
[c] Università di Bologna, Bologna, Italy
[d] Università di Cagliari, Cagliari, Italy
[e] Università di Ferrara, Ferrara, Italy
[f] Università di Firenze, Firenze, Italy
[g] Università di Urbino, Urbino, Italy
[h] Università di Modena e Reggio Emilia, Modena, Italy
[i] Università di Genova, Genova, Italy
[j] Università di Milano Bicocca, Milano, Italy
[k] Università di Roma Tor Vergata, Roma, Italy
[l] Università di Roma La Sapienza, Roma, Italy
[m] Università della Basilicata, Potenza, Italy
[n] LIFAELS, La Salle, Universitat Ramon Llull, Barcelona, Spain
[o] Hanoi University of Science, Hanoi, Viet Nam
[p] Massachusetts Institute of Technology, Cambridge, MA, United States

JHEP02(2013)106